OUTLINE

- B fields in quasars and BL Lac objects
- Evidence for toroidal/helical B fields
- Superluminal speeds
- Core rotation measures
- Circular polarisation

Gomez, Marscher, & Alberdi 1999

E+90°

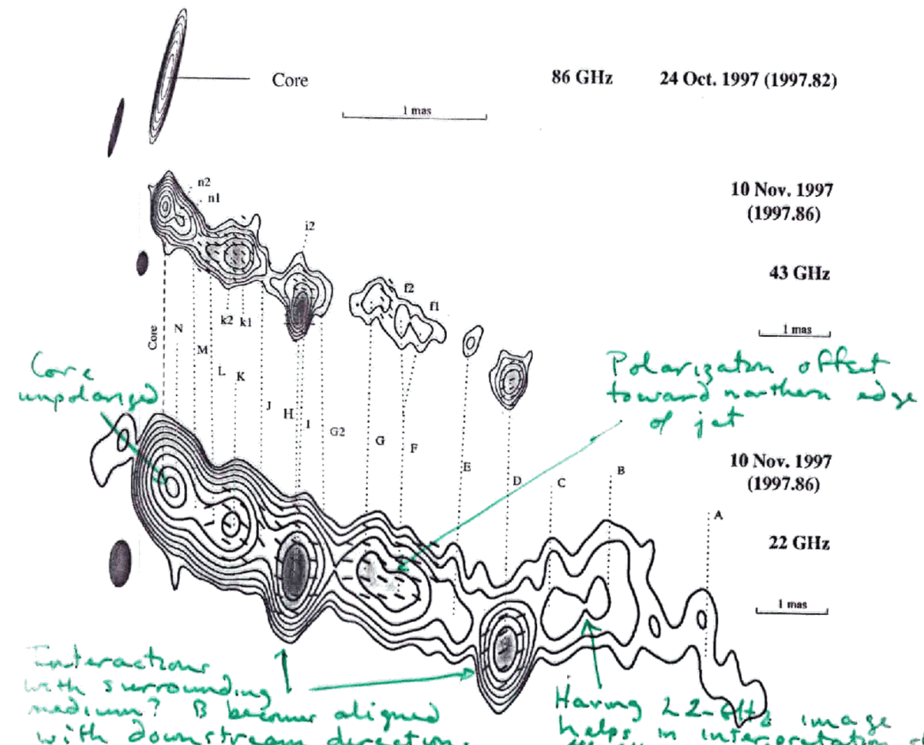

FIG. 1.—VLBI images of 3C 120 at 86 (*top*), 43 (*middle*), and 22 GHz (*bottom*). Total intensity is plotted as contour maps, while the linear gray scale shows the linearly polarized intensity (22 and 43 GHz only). The superposed bars give the direction of the *magnetic field* vector. For the 86, 43, and 22 GHz images, contour levels are in factors of 2, starting at (noise level) 2%, 0.9%, and 0.5% of the peak intensity of 1.51, 0.54, and 0.48 Jy beam^{-1}, respectively (43 and 86 GHz images contain an extra contour at 90% of the peak). Convolving beams (shown to the lower left of the core of each image) are 0.40 × 0.054, 0.32 × 0.16, and 0.63 × 0.30 mas, with position angles of −13°, −6°, and −4°. Peaks in polarized intensity are 27 and 42 mJy beam^{-1}, with noise levels of 3 and 2 mJy beam^{-1} for the 43 and 22 GHz images, respectively. The epoch and scale of each map are shown on the right (note that 86 GHz map scale is twice that of the other maps).

Opacity corrections were introduced by solving for receiver temperature and zenith opacity at each antenna. Fringe fitting to determine the residual delays and fringe rates was performed for both parallel hands independently and referred to a common reference antenna. Delay differences between the right- and left-handed polarization systems were estimated over a short scan of cross-polarized data of a strong calibrator (3C 454.3). The instrumental polarization was determined by using the feed solution algorithm developed by Leppänen et al. (1995).

The absolute phase offset between right- and left-circular polarization at the reference antenna was determined by VLA observations of the sources 0420−014 and OJ 287 on 1997 November 21 and referenced to an assumed polarization position angle of 33° for 3C 286 and 11° for 3C 138, at both observing frequencies. This provided an estimation of the absolute polarization position angle within 9° and 7° at 22 and 43 GHz, respectively.

3. RESULTS AND CONCLUSIONS

Figure 1 shows the resulting CMVA and VLBA images of 3C 120. Table 1 summarizes the physical parameters obtained for 3C 120 at the three frequencies. Tabulated data correspond to total flux density (S), polarized flux density (P), magnetic vector position angle (χ_B), separation (r), and structural position angle (θ) relative to the easternmost bright component (which we refer to as the "core") and angular size (FWHM). Components in the total intensity images were analyzed by model

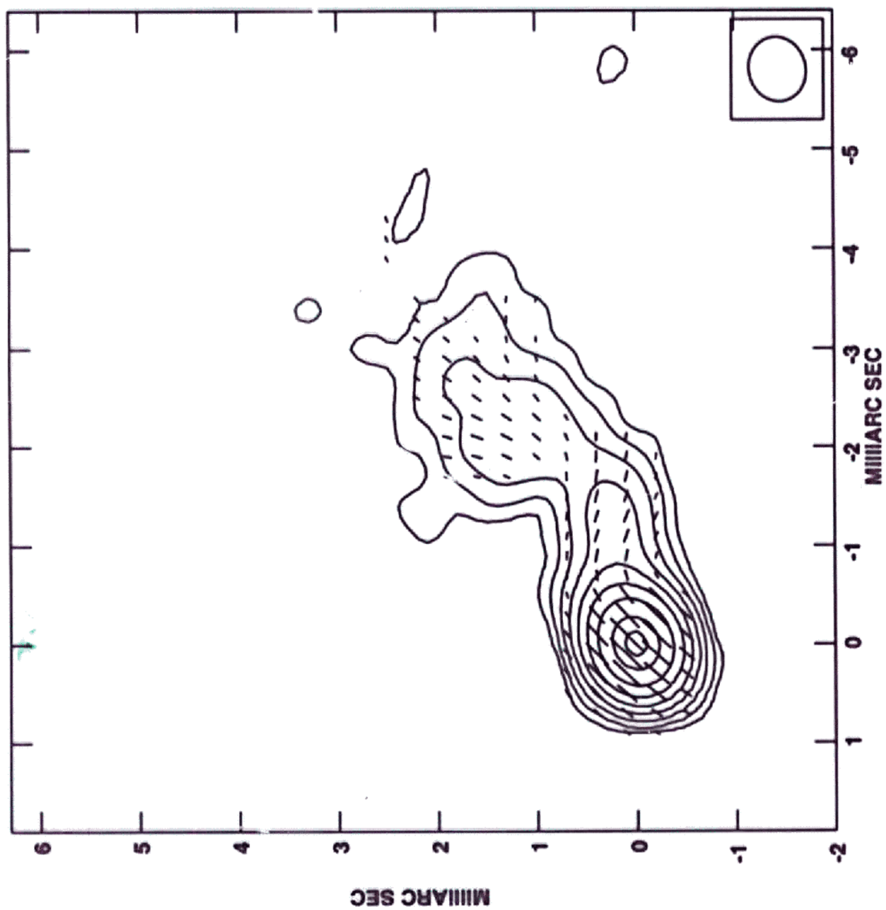
MilliARC SEC

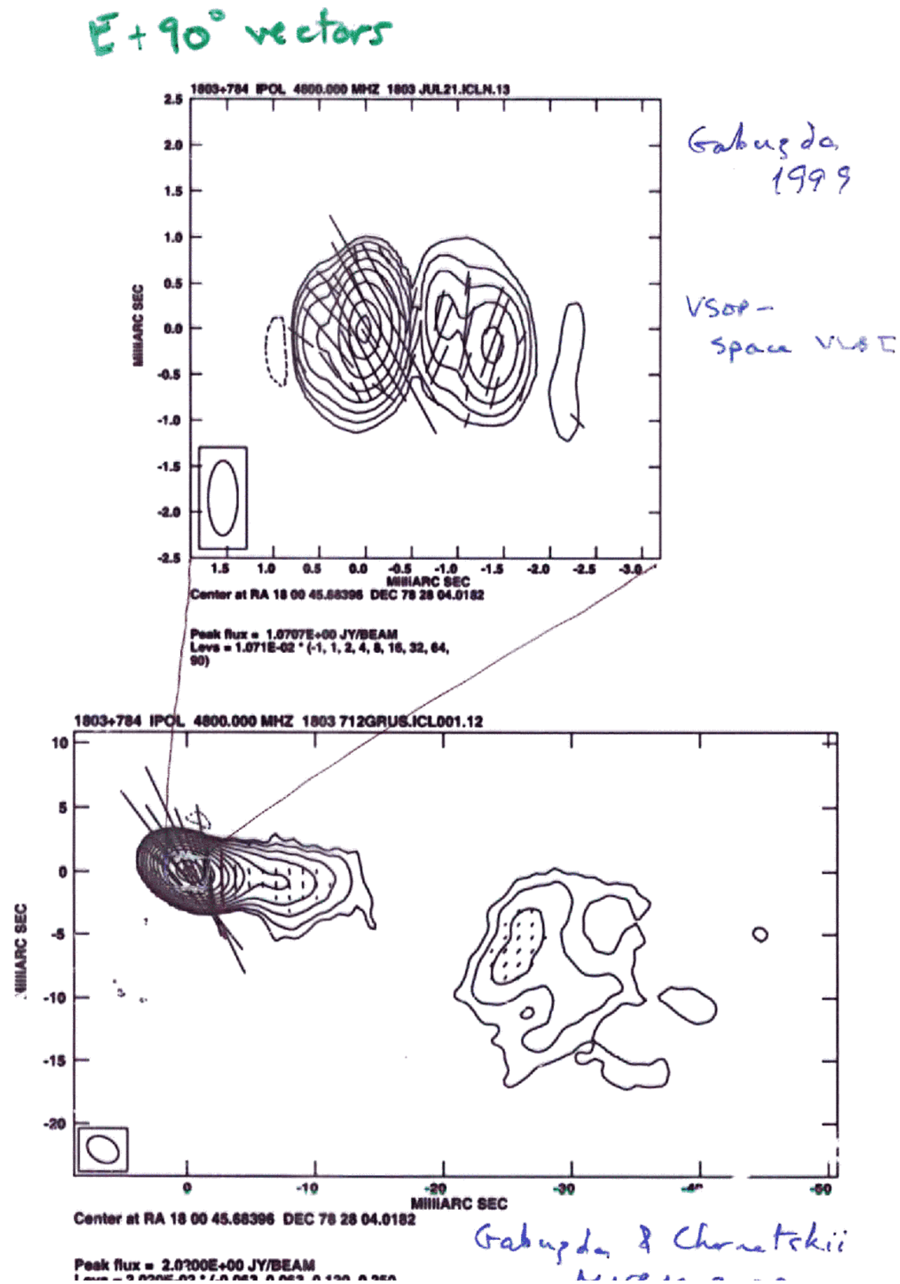
E+90° vectors
1803+784 IPOL 4800.000 MHZ 1803 JUL21.ICLN.13
Gabuzda 1999
VSOP - Space VLBI
MilliARC SEC
Center at RA 18 00 45.68396 DEC 78 28 04.0182
Peak flux = 1.0707E+00 JY/BEAM
Levs = 1.071E-02 * (-1, 1, 2, 4, 8, 16, 32, 64, 90)
1803+784 IPOL 4800.000 MHZ 1803 712GRUS.ICL001.12
MilliARC SEC
Center at RA 18 00 45.68396 DEC 78 28 04.0182
Peak flux = 2.0200E+00 JY/BEAM
Gabuzda & Chernetskii

THEORY (K. Tsinganos, A. Mastichiadis, N. Vlahakis et al.)

- Experience in constructing steady analytical 3-D models of MHD winds and jets (relativistic & nonrelativistic).
- Experience in constructing self-similar solutions, demonstration of the role of the critical surfaces, developing criteria for the collimation of MHD outflows, the asymptotics of collimated and cronical solutions, the structural stability of MHD outflows and the efficiency of magnetic acceleration.
- Numerical simulations of time-dependent MHD winds/jets, demonstration of magnetic collimation & shock formation, acceleration of relativistic jets. Gamma ray bursts.
- Time-dependent radiative transfer. Spectrum formation from synchrotron, synchro self-Compton and external Compton processes. Particle acceleration in shock waves and coupling with radiation. Application to blazars and gamma-ray bursts.

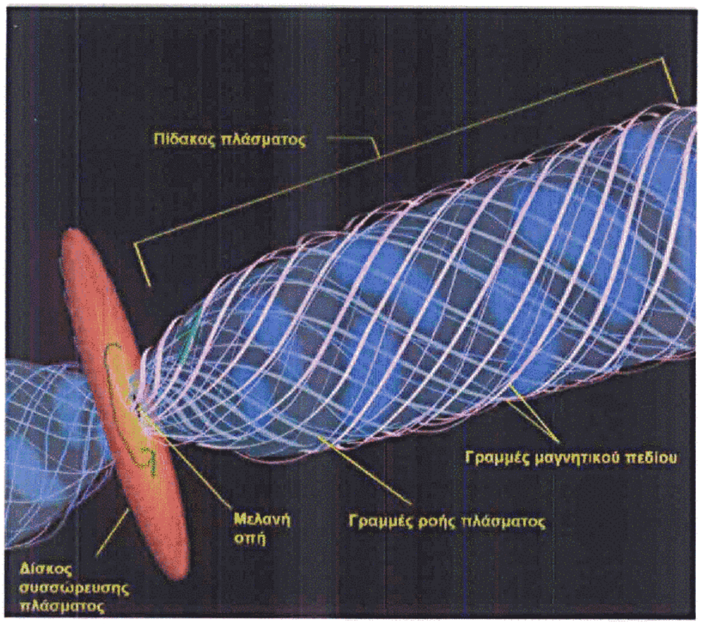

If we are observing toroidal or helical B fields associated with these jets, this may give rise to Faraday-rotation gradients across the jets, due to changing line-of-sight B field component:

intrinsic pol. angle

$$\chi_{obs} = \chi_0 + RM \cdot \lambda^2$$

"rotation measure" $\propto \int n(s)\vec{B}(s)\cdot d\vec{s}$

element of path along LOS

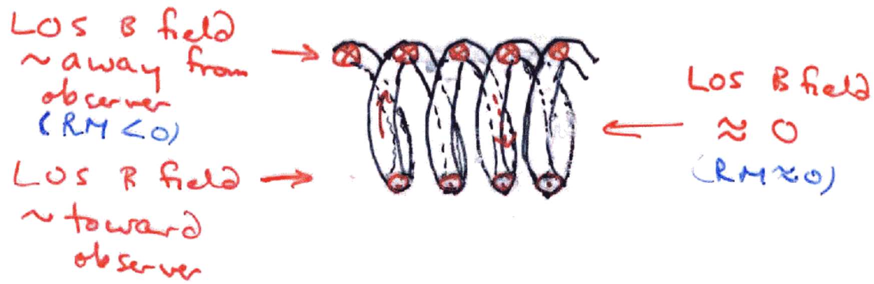

Dependence of RM profile on pitch angle

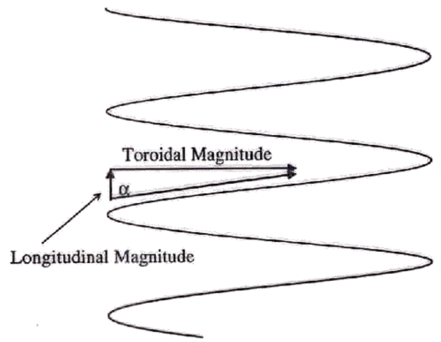

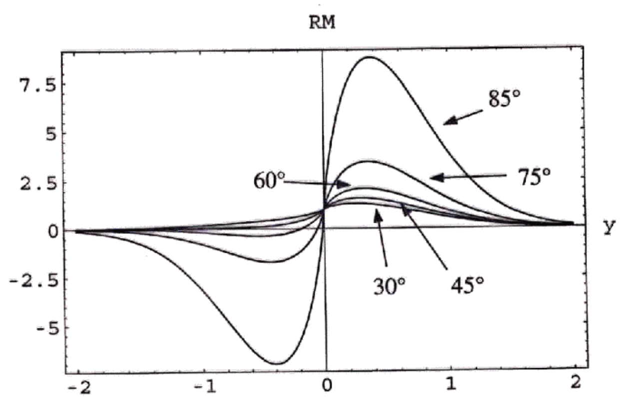

Dependence of RM profile on viewing angle

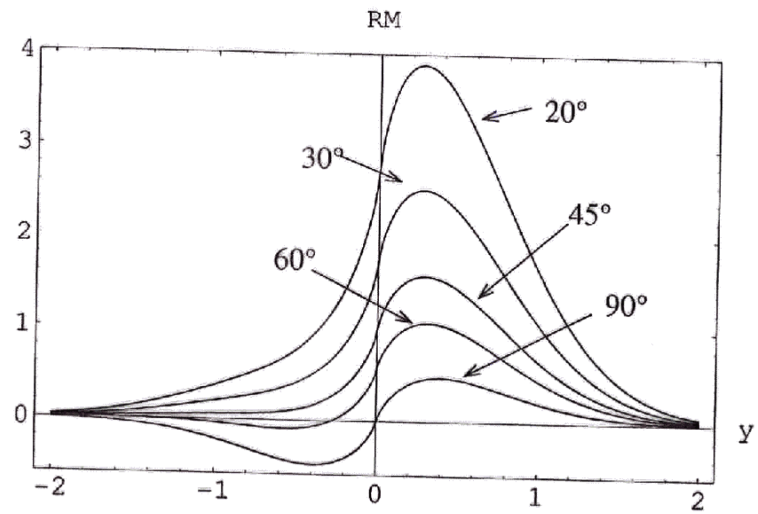

(Viewing angle of 90° in source frame ≈ viewing angle of $\sim \frac{1}{\gamma}$ in observer's frame)

10 K. Asada et al. PASJ 2002

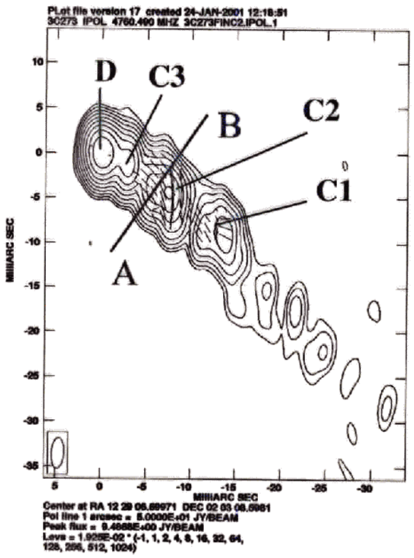

Fig. 2.

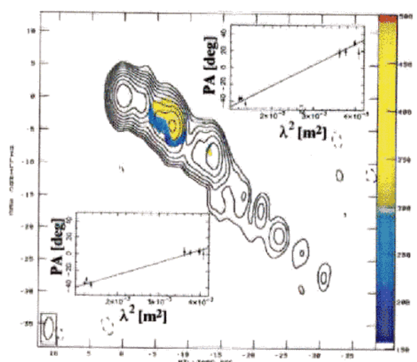

Fig. 3.

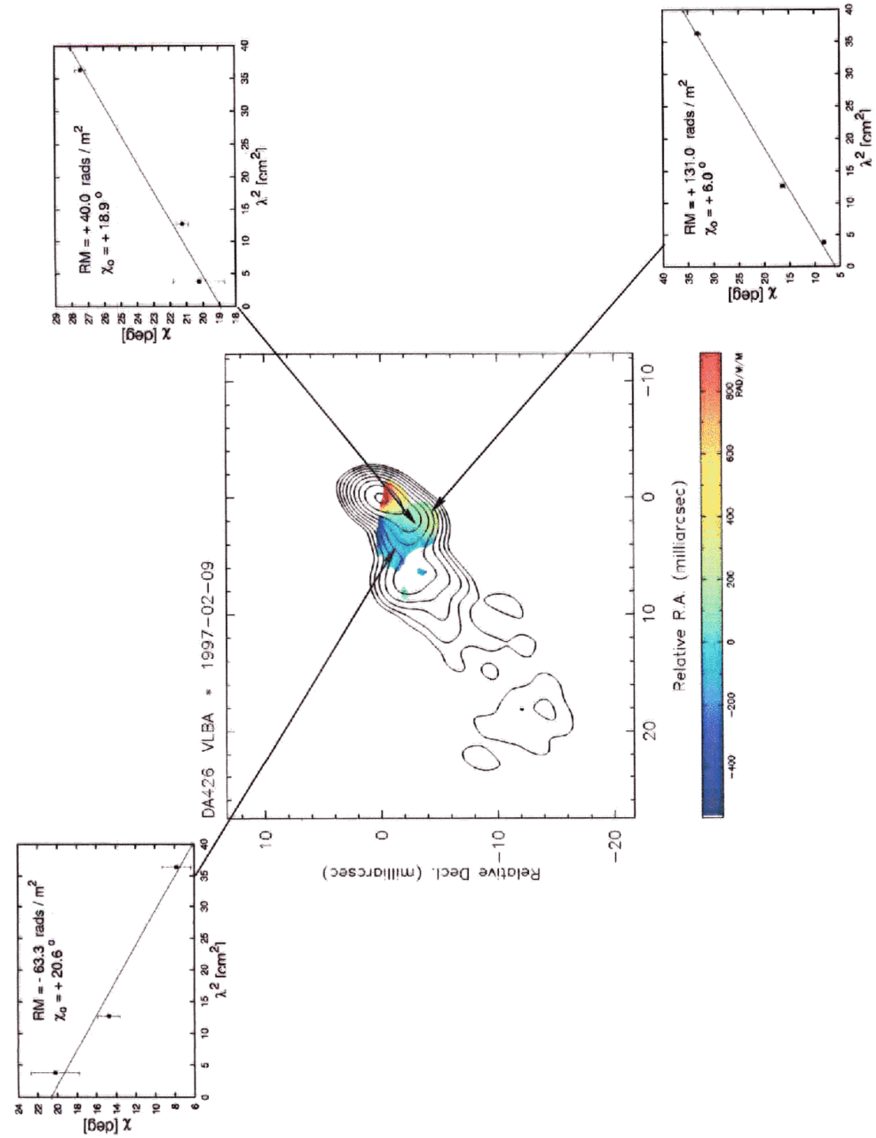

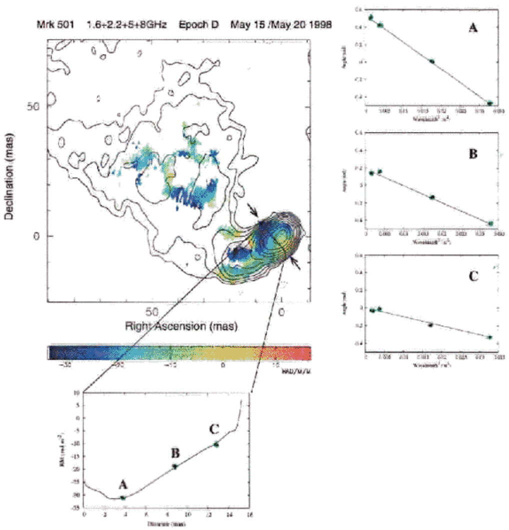

Figure 5.4: Rotation Measure map constructed from D epoch 1.6, 2.2, 5 & 8 GHz data. Both maps were first convolved with a beam FWHM 6.0 x 4.5 mas, PA = $-10°$ (corresponding to the 1.6GHZ beam size). The contours of total intensity at 1.6GHz are superimposed. Levels increase by a factor of 2 at each contour, from the lowest level of 0.7mJy. Plots show the profile of the rotation measure distribution across the slice indicated by arrows (bottom), and the fits obtained at points along the slice (right).

resulting in small errors. The line along which the maximum RM gradient is detected changes orientation along the jet. This supports the presence of a curved jet trajectory, although the features described in the previous chapter cannot be identified in the RM

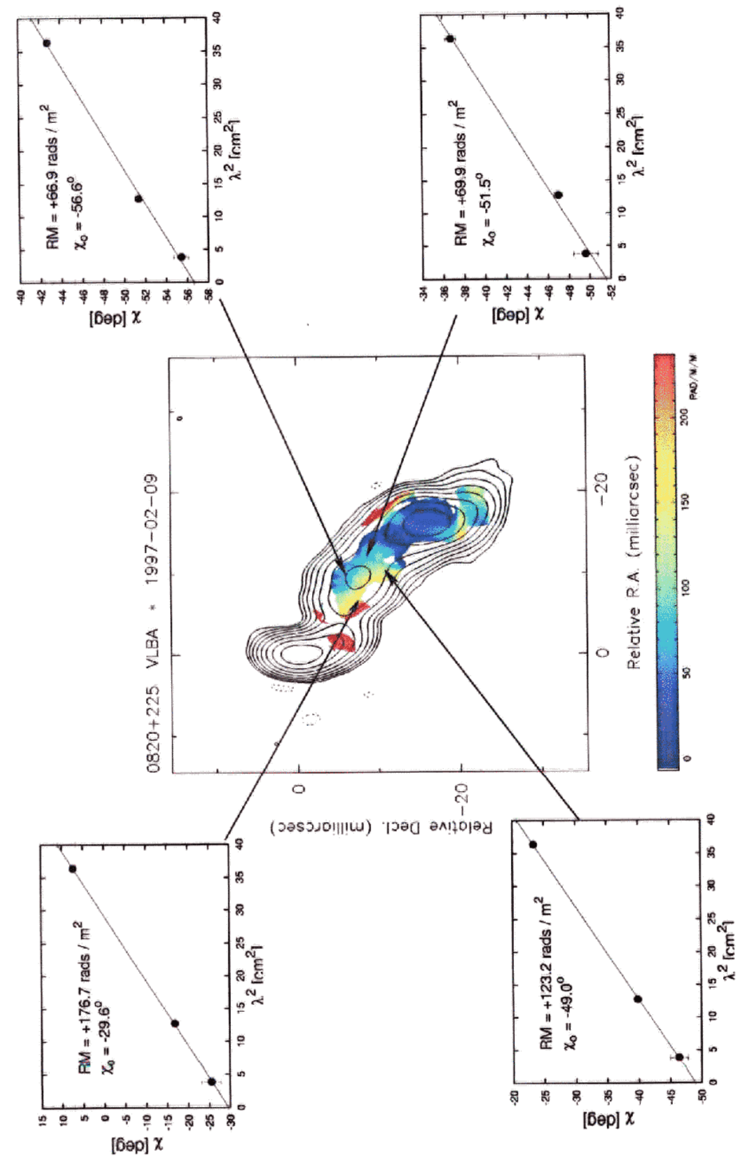

E + 90°

Gabuzda, Pushkarev & Carroll MNRAS, 2000

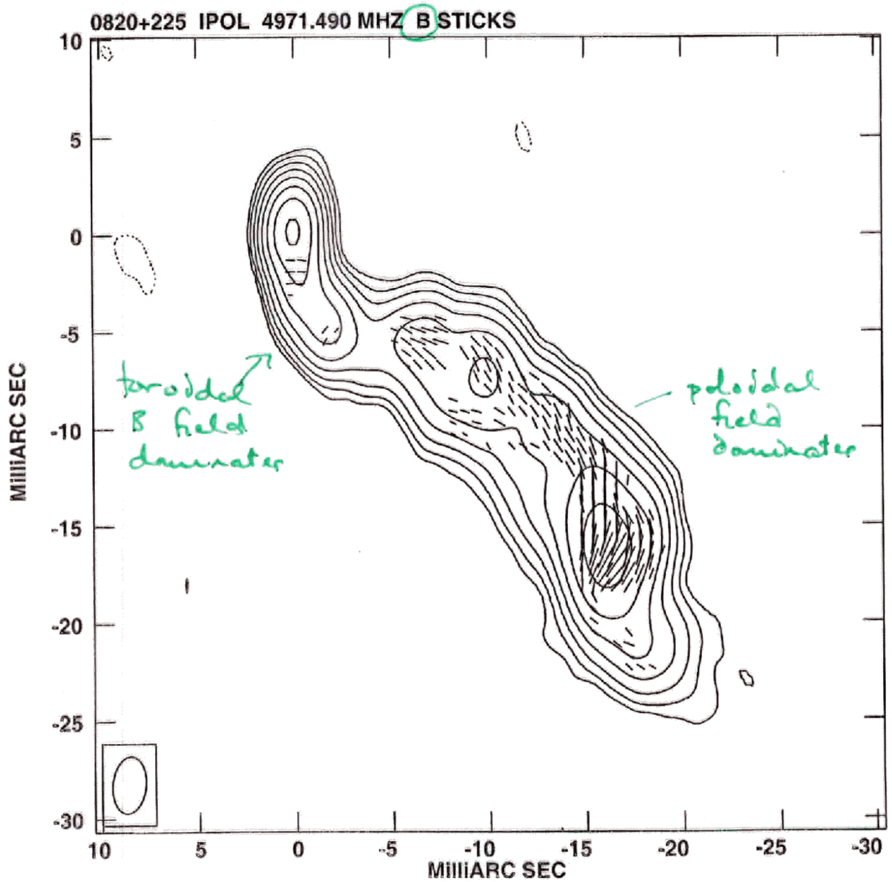

Pushkarev et al 2005 MNRAS

Mrk 501?

E vectors

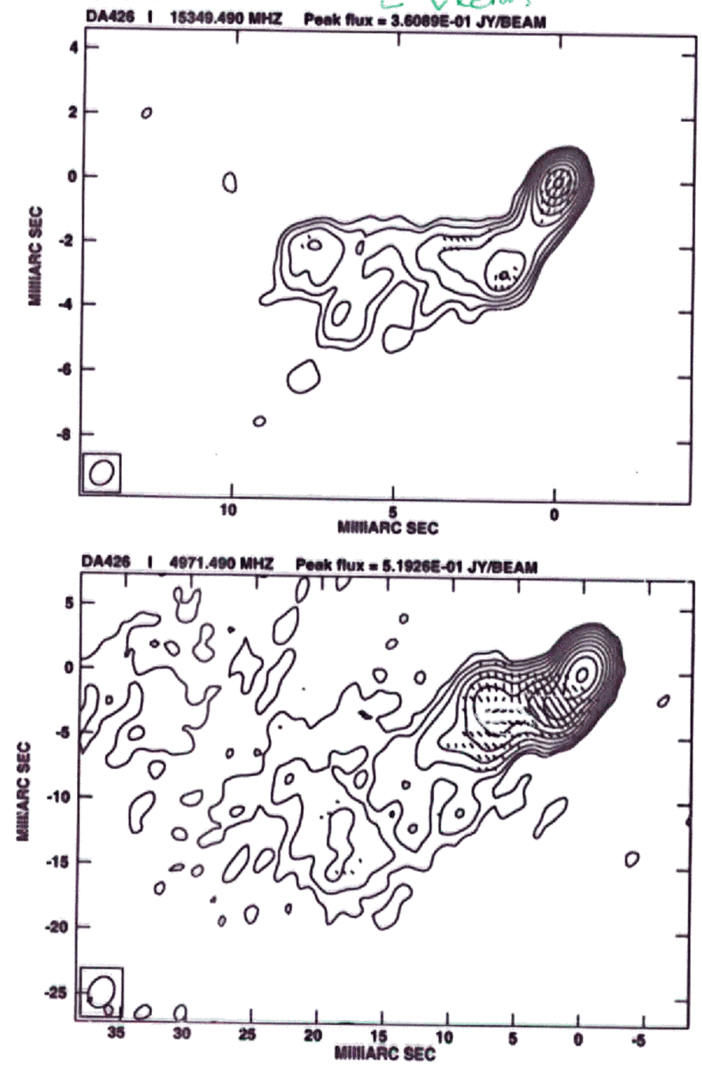

Croke & Gabuzda in prep.

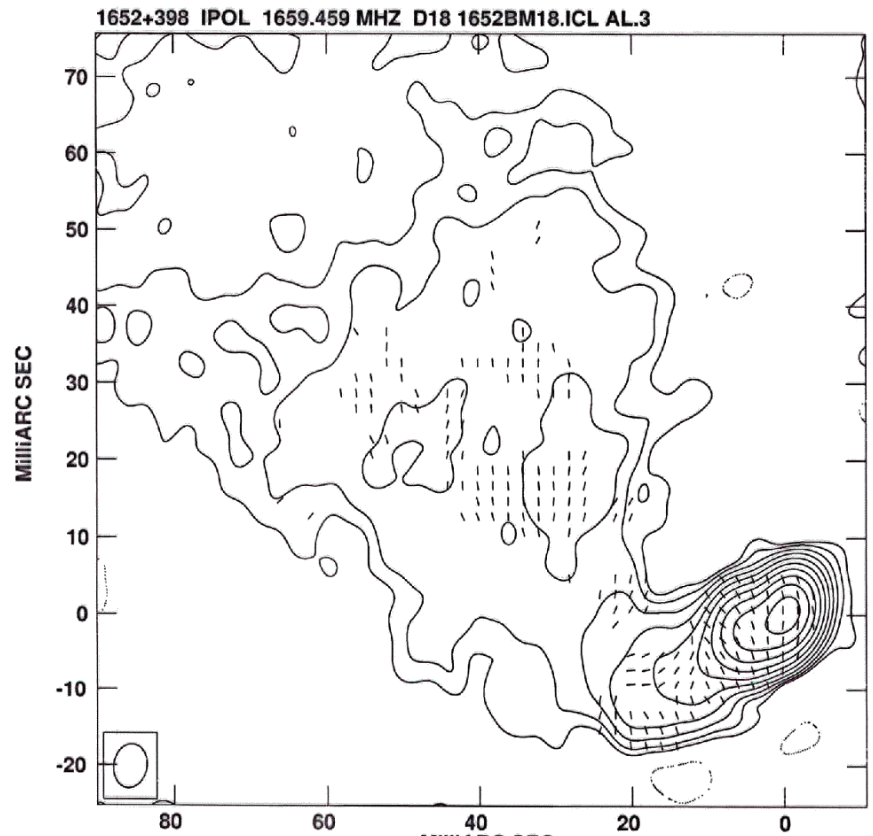

Center at RA 16 53 52.21671 DEC 39 45 36.6091
Pol line 1 arcsec = 1.0000E+03 RATIO
Rotated by -90.0 degrees
Peak flux = 5.1900E-01 JY/BEAM
Levs = 1.000E+00 * (-0.001, 0.001, 0.001, 0.003, 0.006, 0.011, 0.022, 0.045, 0.090, 0.179, 0.358)

Corrected for local Faraday rotation

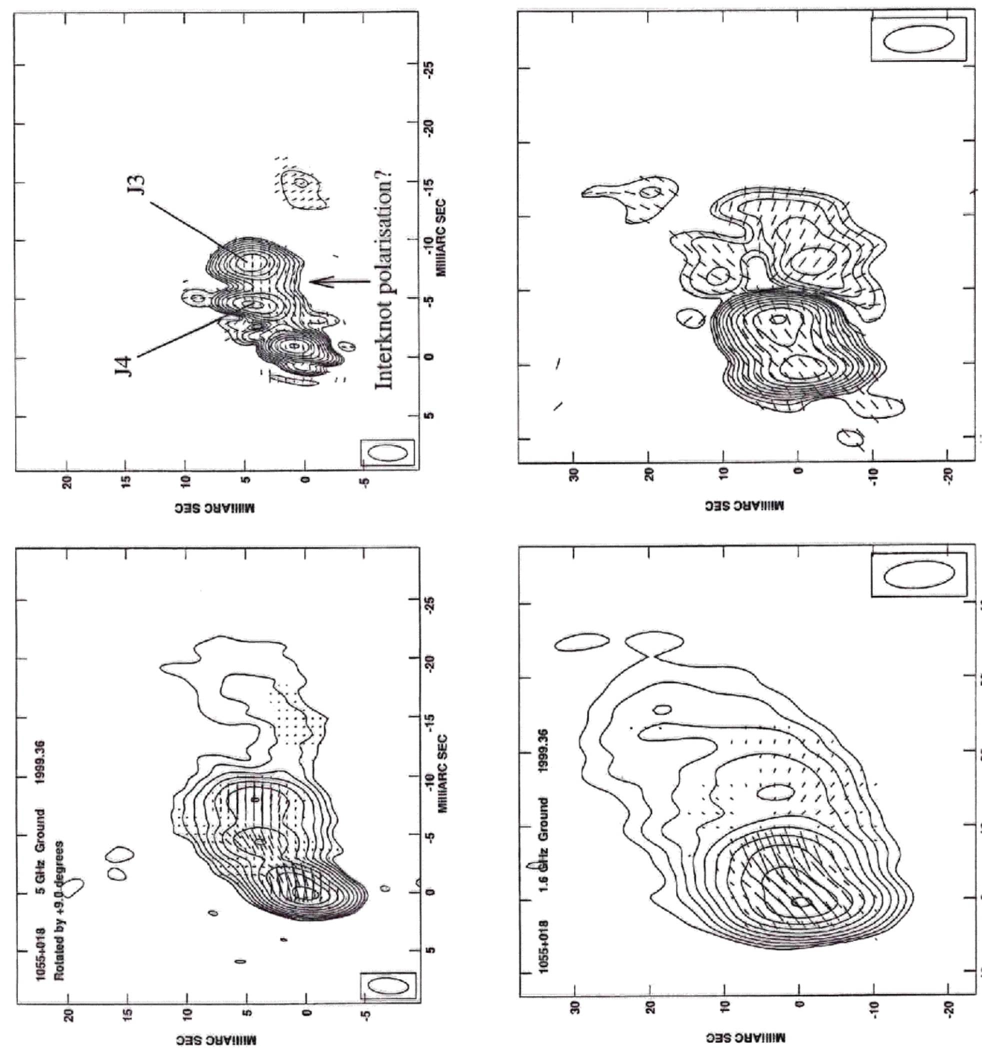

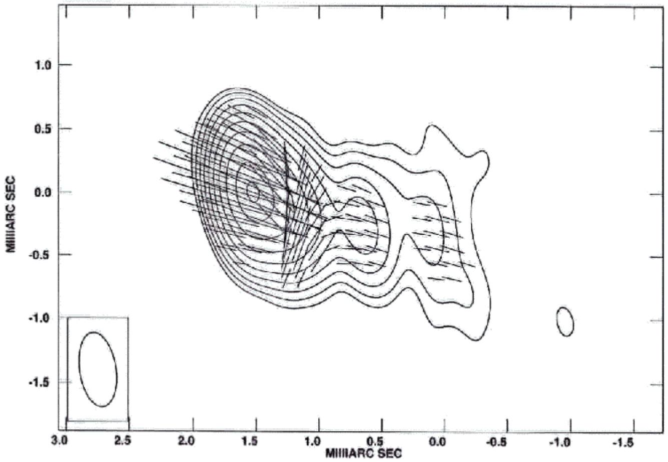

1.3 cm VLBA image of OJ287.

Gabuzda & Gómez 200

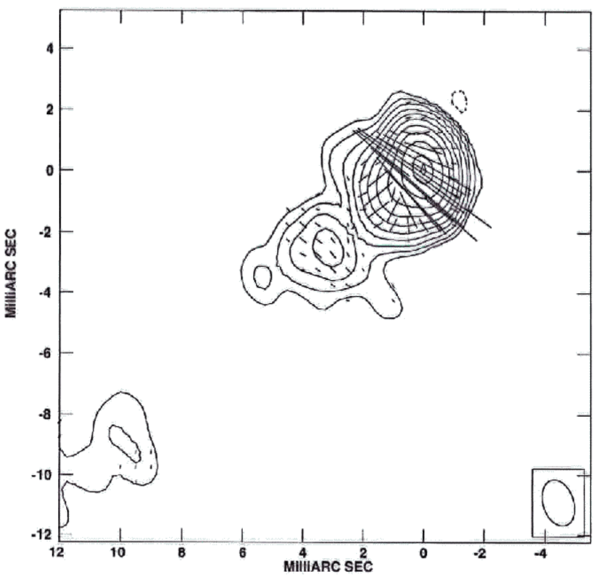

6 cm VLBA image of 1418+546.

Pushkarev et al 2005

Kellermann et al 2004

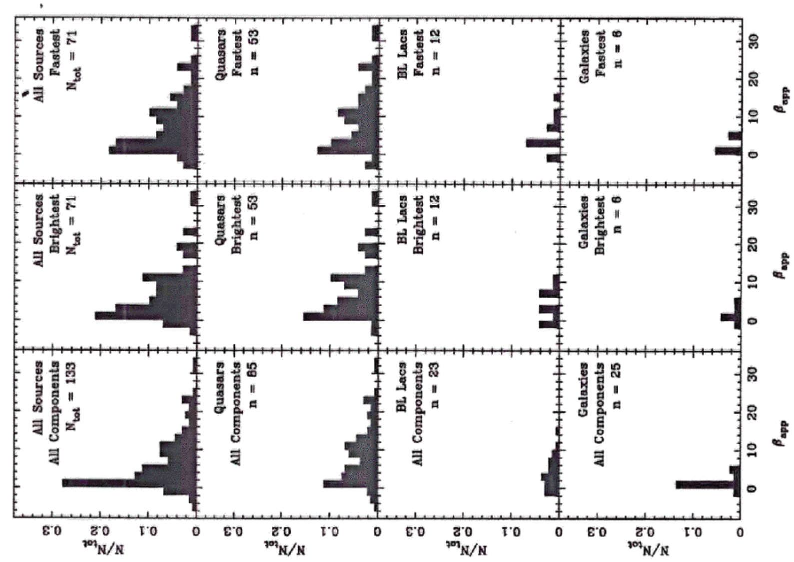

FIG. 5.— Same distributions as in Figure 4 except only those sources contained in our representative flux density-limited sub-sample are included.

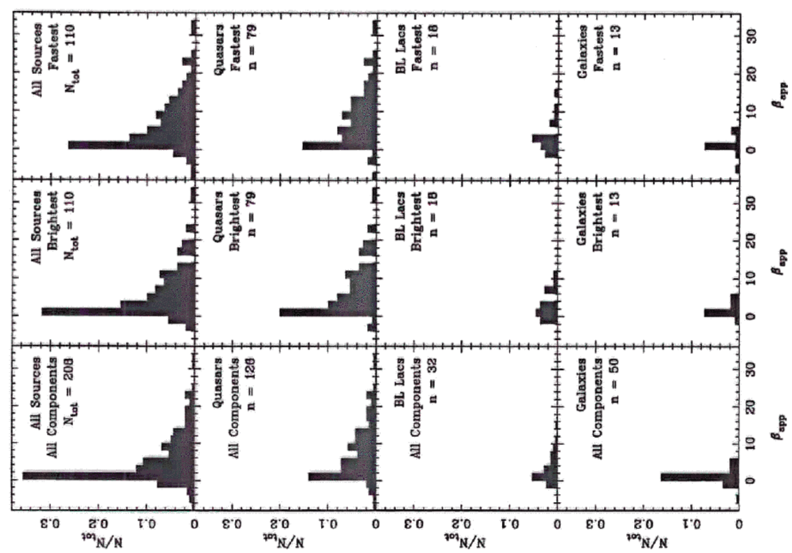

FIG. 4.— Distribution of the apparent linear velocity in all sources with a quality code 'E' or 'G' and which have measured redshifts. The left hand column displays the distribution for all individual features which we have observed. Distributions in the center and right columns show only one feature per source, the brightest or the fastest respectively. Sources are divided by optical class in the second, third and fourth rows of the figure.

Jets are not ballistic structures

Kinematics of Jets – III 11

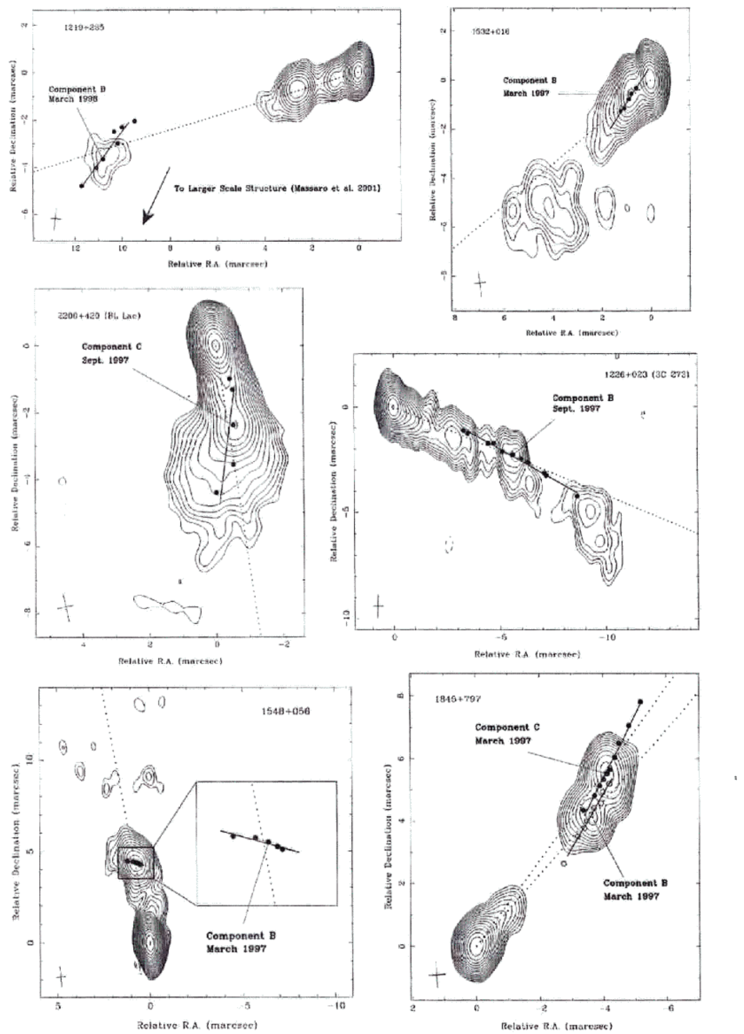

FIG. 7.— Selected images of sources with jets that show non-ballistic component motion. Measured component positions for each epoch are superimposed on the images along with the vector motion (solid lines) in the RA – Dec plane. Dashed lines represent the mean structural position angles, $\langle\vartheta\rangle$, for each component.

Could systematic difference in SL speeds for quasars and BL Lac objects have implications for B_ϕ / B_z ?

Taylor 2000

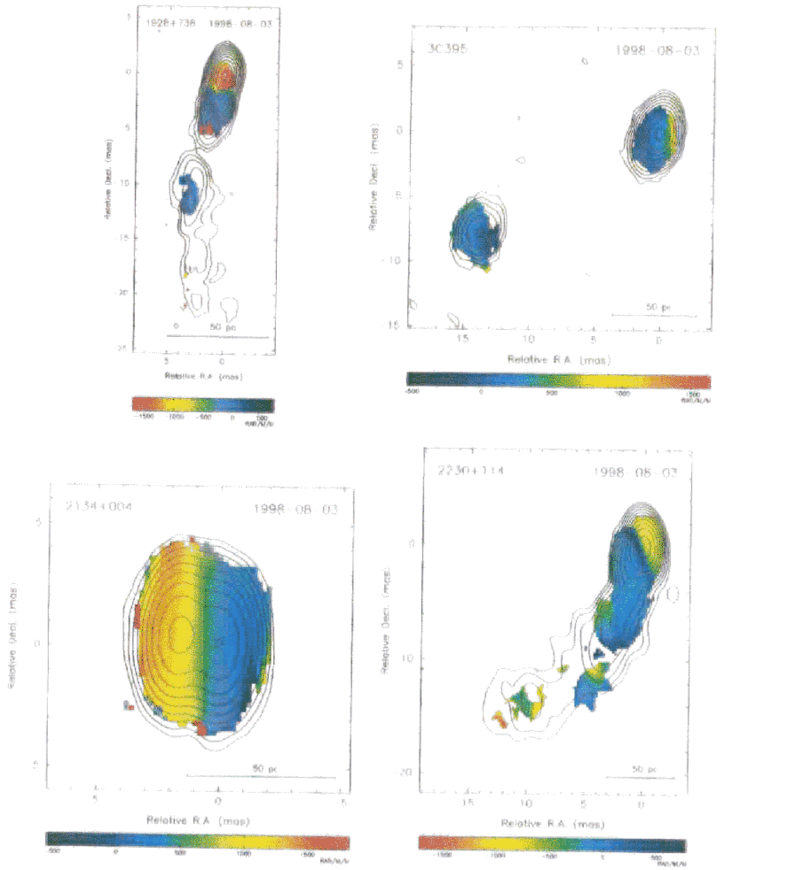

FIG. 6 Rotation measure images of 1928+738, 3C 395, 2134+004, and 2230+114 with contours of total intensity superimposed. Contours are as in Figs 1–4.

According to unified schemes (see, for example, the review by Antonucci 1993), core-dominated quasars are viewed such that the jet axis makes only a small angle to the line of sight and they therefore exhibit one-sided jets, apparent superluminal motions, and broad optical emission lines. While jet components are within ~100 pc of the center of activity, they are viewed through ionized gas which acts as a Faraday screen. Once the jet components move farther from the nuclear environment, the RM rapidly drops.

An observer looking at an AGN nearly edge-on through the denser, multiphase disk would likely see a galaxy with narrow optical emission lines and symmetric parsec-scale radio structures. The much smaller (~1 pc) broad line region is hidden from view by the molecular disk. While the cores of lobe-dominated FR II radio galaxies (generally unified with quasars) have not yet been observed with VLBI polarimetry, there is another class of bright sources known as compact symmetric objects (CSOs) that are likely to be youthful versions of FR II radio galaxies (Readhead et al. 1996). For the CSOs, which often have intrinsic sizes less than ~100 pc, all the components will be viewed through a dense multiphase medium, and extremely high RMs

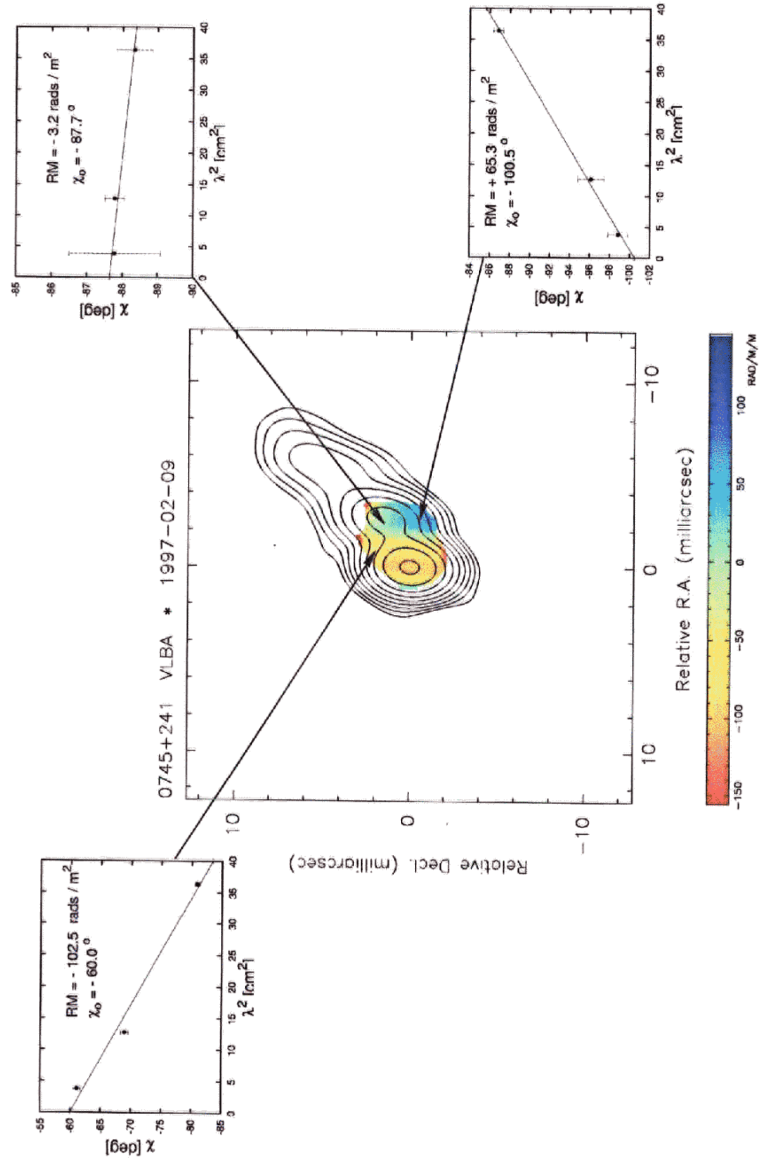

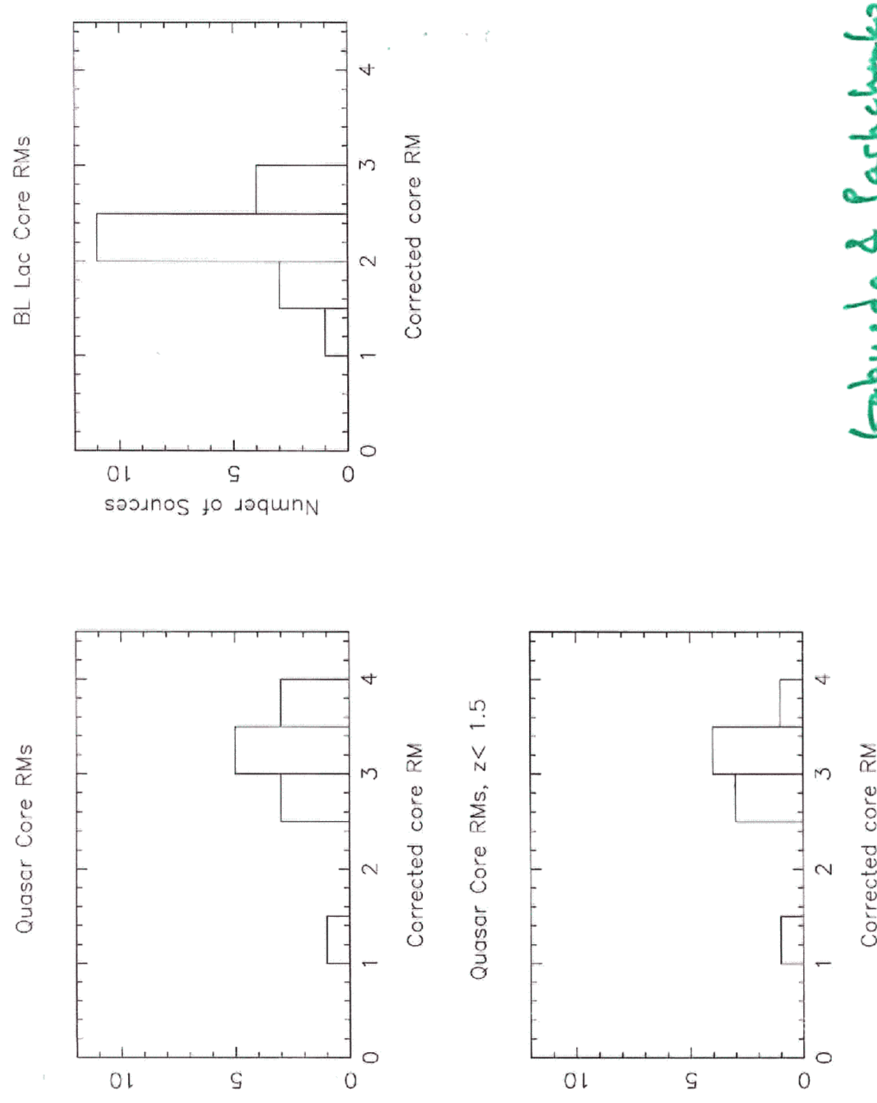

Gabuzda & Pashchenko, in prep.

Lower core rotation measures for BL Lac objects

⇒ fewer free electrons

⇒ lower matter density

and/or

fewer ionising photons

Could a lower matter density in BL Lacs lead to a lower accretion rate, and thereby lower outflow speeds?

FR I radio galaxies may be more polarized (less depolarized) than FR II galaxies

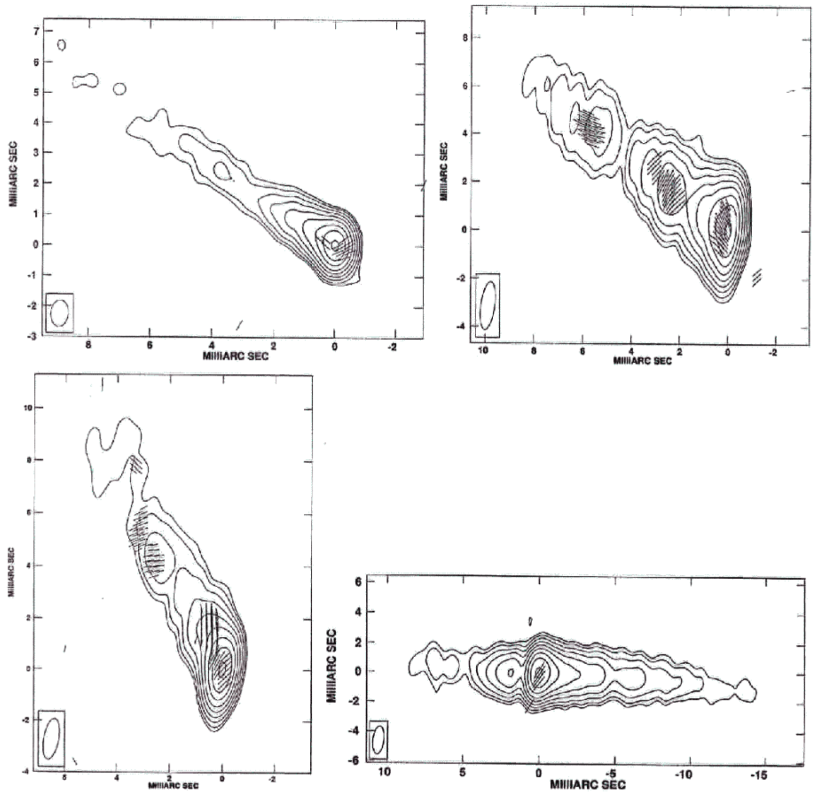

Figure 1: Total intensity maps with polarization electric vectors superimposed. *Clockwise from top left:* (1) FRI radio galaxy 3C 66B, peak surface brightness = 118.2 mJy beam^{-1}; (2) 3C 78, peak surface brightness = 285.9 mJy beam^{-1}; Both these FRIs show a transverse B-field in their inner jets, similar to that observed in BL Lac objects. (3) 3C 270, peak surface brightness = 165.3 mJy beam^{-1}; (4) 3C 264, peak surface brightness = 136.3 mJy beam^{-1}. Contours are in percentage of the peak and increase in steps of × 2, lowest contour = -0.35% of peak, in all the maps.

Kharb et al. in prep

Circular polarisation on Parsec Scales

- In core or innermost jet
- ~ a few tenths of a per cent
- evidence for sign consistency over time

Theoretically, spectrum can give info about mechanism

- intrinsic synchrotron
- linear-to-circular conversion in thermal or relativistic plasma

But still very little info.

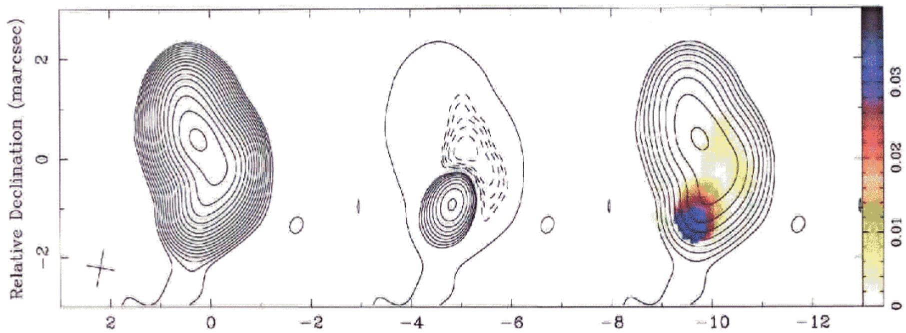

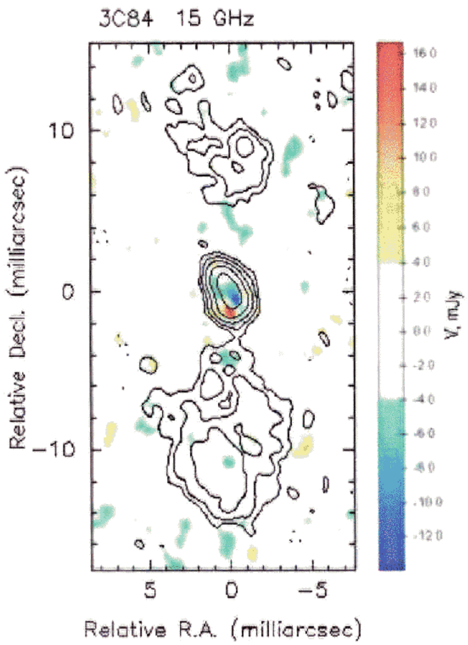

Max I: 4.12 Jy/beam
Contours (%): −0.16 0.16 0.64 2.56 10.24 40.96 40.96 40.96 40.96

Max V: 16.7mJy/beam (0.41% I)
Min V: -13.9mJy/beam (-0.34% I)

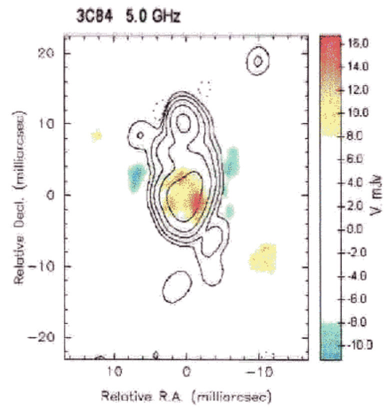

Max V: 16.7 mJy/beam V/I (Vmax): 0.89 %
Max I: 3640 mJy/beam
Contours (%): −0.16 0.16 0.64 2.56 10.24 40.96

Рис. 5.3а. Карта КП 3C84 на 5 ГГц, полученная методом нулевой поляризации. Сигнал КП искажен и имеет противоположный истинному знак.

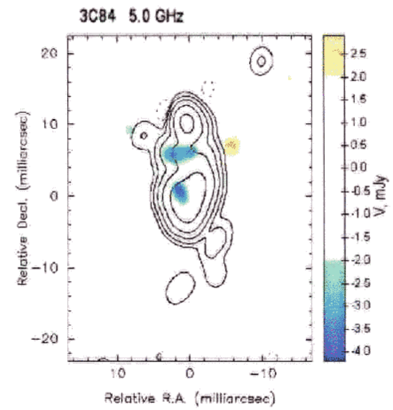

Min V: -4.2 mJy/beam |V|/I (Vu,max): 0.91 %
Max I: 3640 mJy/beam |V|/I (Vl,max): 0.14%
Contours (%): −0.16 0.16 0.64 2.56 10.24 40.96

Рис. 5.3б. Карта КП 3C84 на 5 ГГц, полученная методом переноса поправок.

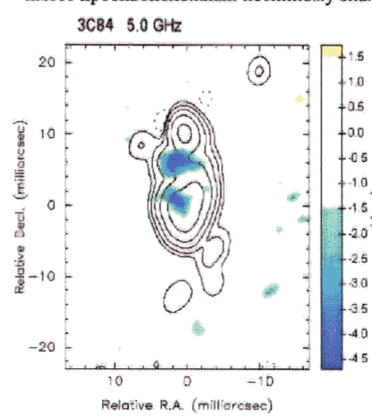

Min V: -4.7 mJy/beam |V|/I (Vu,max): 1.00 %
Max I: 3640 mJy/beam |V|/I (Vl,max): 0.16 %
Contours (%): −0.16 0.16 0.64 2.56 10.24 40.96

Рис. 5.3в. Карта КП 3C84 на 5 ГГц, полученная методом переноса поправок с последующим применением метода раздельной калибровки. Карта сопоставима с результатом Homan&Wardle (рис. 5.3г.)

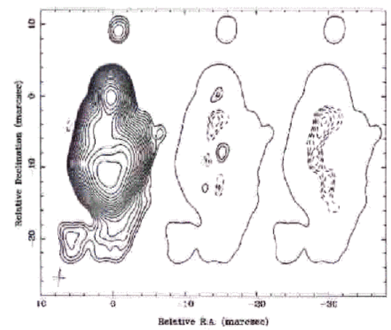

Рис. 5.3г. 3C84 на 5 ГГц из частной переписки Слева – карта интенсивности. В центре- карта КП, полученная методом нулевой поляризации. Справа – карта КП, полученная модифицированным методом нулевой поляризации, максимум соответствует потоку 4 mJy/beam Контуры на картах КП проведены с интервалом √2 с нижним уровнем 1 mJy/beam.

41

SUMMARY

- First firm + direct observational evidence for toroidal (helical?) B fields in AGN jets
  - → "winding up" of seed field
  - → the jets should carry current
  - → the jets are fundamentally electromagnetic structures
- Superluminal speeds are systematically lower in BL Lac objects (weak optical lines) than in quasars (strong optical lines)
- Core Faraday rotation is lower in BL Lacs than in quasars

Can this information be tied together?

Lower matter density in BLs
→ lower accretion rate
→ lower outflow speeds
→ higher B_ϕ/B_z

(Lower accretion rate may also lead to lower flux of ionising photons from accretion disk)

Circular polarization must be tied in too!